Received: 18 December 2023 | Revised: 22 August 2024 | Accepted: 24 August 2024

DOI: 10.1002/mp.17420

RESEARCH ARTICLE

MEDICAL PHYSICS

3D printing of realistic body phantoms: Comparison of measured and simulated organ doses on the example of a CT scan on a pregnant woman

Patrizia Kunert[1] | **Helmut Schlattl**[1] | **Sebastian Trinkl**[1] | **Edilaine Honorio da Silva**[1] | **Detlef Reichert**[2] | **Augusto Giussani**[1]

[1]Department of Medical and Occupational Radiation Protection, Federal Office for Radiation Protection, Oberschleißheim, Germany

[2]Department of Physics, Martin-Luther University Halle-Wittenberg, Halle (Saale), Germany

Correspondence
Patrizia Kunert, Externe und interne Dosimetrie, Biokinetik, Abteilung für medizinischen und beruflichen Strahlenschutz, Bundesamt für Strahlenschutz, Ingolstädter Landstr. 1, D-85764 Oberschleißheim, Germany.
Email: pkunert@bfs.de

Abstract

Background: Medical examinations or treatment of pregnant women using ionizing radiation are sometimes unavoidable. In such cases, the risk of harm to the embryo and fetus after exposure to ionizing radiation must be carefully estimated. However, no commercially available anthropomorphic body phantoms of pregnant women are available for dose measurements. A promising possibility for the production of body phantoms for patient groups that are not adequately represented by the phantoms of reference persons is 3D printing. However, this approach is still in the evaluation phase.

Purpose: To print the abdomen of a woman in the late stage of pregnancy and compare the dose distribution measured using thermoluminescence dosimeters (TLDs) in the printed phantom for two different computed tomography (CT) protocols with the corresponding results of Monte Carlo simulations on voxel models of the pregnant woman.

Materials and methods: The physical phantom was produced through multi-material extrusion printing using different print materials identified in previous studies to simulate homogeneous soft tissues and the mean compositions of maternal and fetal bones. The 3D printed abdomen was combined with a conventionally produced anthropomorphic female phantom to obtain a whole-body phantom of a pregnant woman. Dose values resulting from two different CT scans acquired at tube voltages of 80 and 120 kV were measured using TLDs positioned in the physical phantom and cross-validated with the results of Monte Carlo simulations performed for two different voxel models. The first was a voxelized model of the produced phantom itself and the second a realistic digital model of a pregnant woman. Representative CT values of the materials used in the printed phantom were determined from the acquired CT images.

Results: The CT values of maternal and fetal tissue structures in the phantom are comparable to CT values of real human tissues. The difference between most organ doses measured in the 3D printed phantom and simulated in the voxel models was below 20% and equivalent within the measurement uncertainties. Only the dose to the fetal head was up to 50% higher and not equivalent for the realistic model and the 80 kV-protocol. As expected, the agreement was better for the voxelized than for the realistic model. For both models a slight

energy dependence was observed, with larger deviations for the 80-kV protocol especially for organs located in the pelvic region.
Conclusion: Individualized physical body phantoms, such as that of a pregnant woman, can be produced using 3D printing. The good agreement between measured and simulated doses to the fetus cross-validates both dosimetric methods. Therefore, this study demonstrates the suitability of 3D printing phantoms for patients not adequately represented by commercially available body phantoms of reference persons.

KEYWORDS
3D printing, anthropomorphic phantoms, pregnancy, radiation protection

1 | INTRODUCTION

The exposure of embryos and fetuses to ionizing radiation can lead to different stochastic and deterministic radiation effects, depending on the phase of gestation.[1,2] Nevertheless, clinically indicated medical radiation exposures may still be performed on pregnant patients if the radiation risks for the embryo or fetus are lower than the risks for the mother when not adequately treated.[3]

The exposure of the unborn must be determined carefully to assess the radiation risks of the unborn before an intentional or after an unintentional exposure of a pregnant patient by diagnostic or interventional x-ray procedures. In the early phase of pregnancy, doses to the embryo can be measured or computed using a physical or digital body phantom of a non-pregnant reference woman, using the uterine dose as surrogate quantity.[4,5] However, in the later stages of pregnancy, this method is no longer appropriate. Instead, physical or virtual phantoms that represent the changed anatomical situation must be used.

Various virtual pregnancy models are available as mesh-type or voxel-type computational models. The mesh-type models are often not strictly based on tomographic data sets of pregnant patients because organs can be constructed using computer-aided design (CAD) programs according to the masses and volumes given in the literature.[6–9] This allows a certain flexibility regarding the position and shape of organs, which enables the construction of different phantoms in relation to the week of pregnancy and the position of the fetus. Owing to this flexibility in the design of mesh-type phantoms, the estimation of fetal doses by Monte Carlo simulations is a commonly used method.[10–13] However, details of the imaging systems required for Monte Carlo simulations are often unknown, such as the characteristics of the bowtie filter in computed tomography (CT) systems.

In contrast, measurements performed in physical phantoms at clinical imaging devices reflect the actual exposure situation of the patient, including all technical details affecting the exposure (e.g., radiation quality and aperture systems). However, this method requires physical anthropomorphic phantoms that realistically represent a patient's anatomy and tissue composition. There are currently no commercially available phantoms for pregnant women. As a solution, individualized setups based on conventional non-pregnant female phantoms are used; for example, adding gelatin boluses or other tissue-equivalent materials to approximate the stature of a pregnant woman at different gestation weeks.[14–20] In other studies, entire phantoms based on patient data or virtual models were produced, for example, by molding technologies.[21–23] Fetal structures were not considered, and the uterus dose was used to estimate the dose to the fetus in all these phantoms.

Three-dimensional printing technology is an easy and cost-effective approach for the production of realistic phantoms. In previous studies, we produced phantom components using multi-material extrusion technology and validated them by comparison with conventionally produced phantoms.[24] With this technology, thermoplastic filaments are extruded through a heated print head into single layers of a 3D object. 3D printing is the most promising method for the production of physical phantoms for patients who are not adequately represented by conventional anthropomorphic phantoms. However, these phantoms are still in the practical evaluation phase.

Therefore, this study aims to validate the concept of individualized 3D printing of realistic body phantoms for the application in x-ray imaging using the example of a pregnant woman.

2 | MATERIALS AND METHODS

2.1 | Production of a compound phantom of a pregnant woman

A commercial anthropomorphic phantom of a slim woman with a height of 173 cm and weight of 55 kg (Atom Model 702; CIRS Inc., Norfolk, USA), consisting of 36 slices from the skull to the femur, each with a thickness of 2.5 cm, was transformed into a pregnancy phantom by replacing slices 23–32 with a 3D

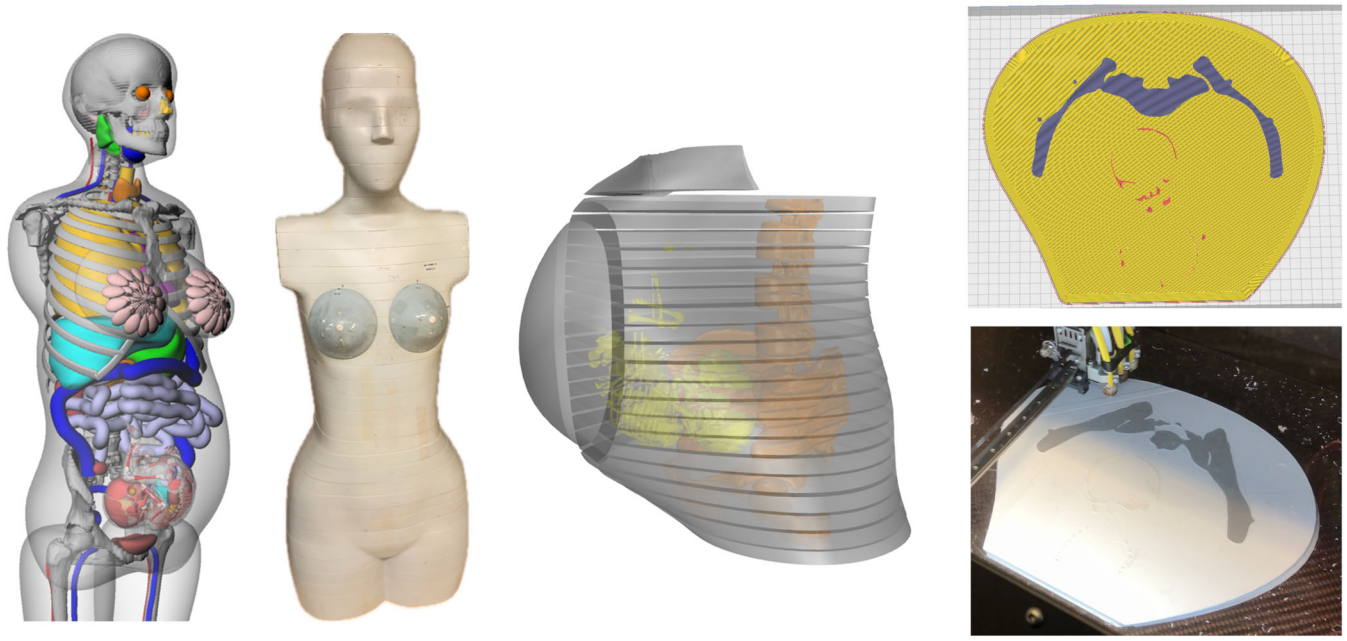

FIGURE 1 Construction of the abdomen of a compound pregnancy phantom consisting of the 3D printed abdomen of a pregnant woman containing the fetus and supplementing parts of a commercially available CIRS phantom. For technical reasons, the front part of the abdomen needed to be printed separately. The major steps (a-d) of the production process are described in the text.

printed abdomen containing a fetus in the 25th week of development.

To generate a template for 3D printing, we used one of the virtual models of pregnant women developed by the University of Florida, representing a 164 cm tall and 65.6 kg heavy woman in the 25th week of pregnancy.[6] This model exists in a mesh and a voxel version. In the following, the virtual model is denoted as UFPF25WK.

The printing process was performed with an industrial multi-material extrusion printer, which can process three different filament materials with three individual nozzles of 0.6 mm in one printing step (3ntr A2 V4; 3ntr, Oleggio, Italy; Figure 1d). Therefore, in the 3D printed abdomen soft tissue, maternal and fetal bones are considered with different materials.

The following steps were taken for the generation of the template:

(1) The abdomen of the virtual mesh model (Figure 1a) was adjusted at the transition between the different phantom parts using CAD software (Rhinoceros 5; Robert McNeel & Associates, Seattle, Washington, USA) to ensure compatibility with the CIRS phantom (Figure 1b), which has a smaller waist and wider hip than the UFPF25WK model. As a result, the waist of the constructed template has a circumference of 800 mm (compared to 890 mm for the UFPF25WK model), while the hips are 930 mm (compared to 780 mm). The circumference of the abdomen itself is 950 mm for both models. Moreover, the bones of the original CIRS abdomen were extracted from CT images using the segmentation software 3DSlicer and inserted in the abdomen template.[25] The CT images were acquired at a clinical CT device (GE Brightspeed; General Electrics, Boston, Massachusetts, USA) in helical scan mode with the following settings: tube voltage, 120 kV; tube current, 50 mA, rotation time, 1.0 s; pitch, 1.375; FOV, 500 mm; reconstructed voxel size, $0.98 \times 0.98 \times 0.63$ mm^3. This way, the compatibility of the maternal spine and femur location in the 3D printed and conventionally produced phantom parts was ensured.
(2) The fetal skeleton was directly imported from the mesh data set of the UFPF25WK model at the same position in the template as in the virtual model.
(3) Templates for the individual phantom slices (Figure 1c) were generated in CAD software using Boolean operations. The thickness of the 3D printed slices was set to 1.25 cm, which is half of the slice thickness of the CIRS phantom (2.5 cm). This allowed for greater flexibility regarding the

TABLE 1 Extrusion filaments and corresponding print settings used for printing the abdomen phantom of a pregnant woman.

Material	Substitute for	Composition	Printing temperature (°C)	Heat bed temperature (°C)	Print speed (mm/s)	Infill density (%)
PLA[a]	Soft tissues	Polylactide	200	60	60	95
Granite/ PLA[b]	Maternal bones	PLA and granite powder	220	60	60	100
Laybrick[c]	Fetal bones	Polymer blend and chalk	190	60	30	100

Manufacturers: a) Filamentworld, Neu-Ulm, Germany; b) Formfutura, Nijmegen, Netherlands; c) CC-Products, Cologne, Germany.

positions of thermoluminescence dosimeters (TLD) for the measurement of organ doses. In total, 20 slices were generated.

(4) Because the width of the abdomen exceeded the effective printing area of the used 3D printer, the frontal part of the abdomen was printed separately. Furthermore, a connecting piece for the upper part of the abdomen and the thorax of the CIRS phantom was printed separately.

Instructions for the printing process were generated in the slicing software Cura 5.0.0 (Ultimaker B.V., Geldermanser, Utrecht, Netherlands), where the individual 3D shapes for soft tissues as well as maternal and fetal bones of each phantom slice were merged and assigned to the individual printing materials and settings. The filaments used and the corresponding print settings are listed in Table 1. Polylactide (PLA) was used as a surrogate for soft tissues. This material has been proven to be soft-tissue equivalent in its attenuation and absorption properties for typical diagnostic x-ray qualities (< 5% difference).[26] The maternal bones were printed with granite/PLA composite, which is meant to represent a mean bone composition. This material was found to have realistic CT values for human bones and was equivalent in the dose absorption to the CIRS bones for a CT examination with 120 kV.[24] However, printing realistic bones remains a critical point, because no adequate tissue-equivalent material is available for the cortical bone.[26] For fetal bones, a chalk-composite material (Laybrick) was used, which has a lower attenuation than the granite/PLA composite[26] and is thus suitable for representing less-calcified bones.

2.2 | Imaging and dosimetry with the compound phantom

The clinical CT mentioned above was used to evaluate the imaging properties of the 3D printed compound phantom and to compare the measured doses with those simulated using voxel models. As shown in Figure 2, the physical compound phantom was placed on the CT table without arms. The phantom slices were secured from slipping using clamping devices provided by CIRS, which do not cause imaging artifacts, and additional adhesive tape.

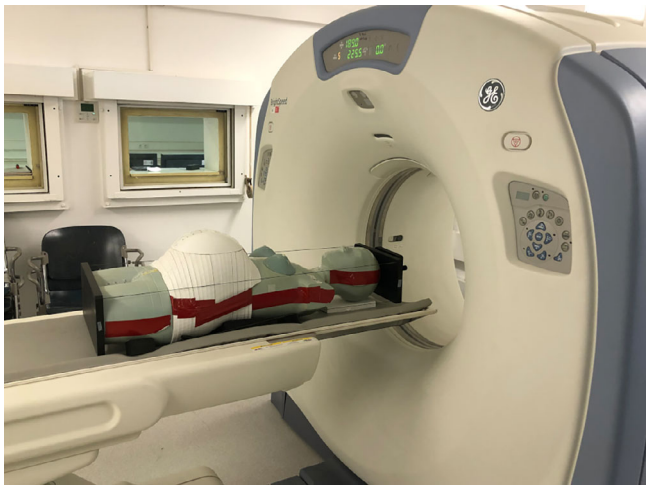

FIGURE 2 Assembly of the compound body phantom, consisting of the 3D printed abdomen and slices of the CIRS phantom attached to both sites, on the CT table.

The trunk (clavicles to femur) of the compound phantom was scanned at two different tube voltages using the parameter settings listed in Table 2. No tube current modulation was used to allow exact dose estimations using the Monte Carlo simulations (described below). Images were iteratively reconstructed with a slice thickness of 2.5 mm using a standard convolution kernel. Mean CT values (in Hounsfield units, HU) and their standard deviations were determined for selected regions of interest (ROI) for both protocols using the ImageJ software.[27] The oval-shaped ROIs were placed over the soft tissue area of the maternal abdomen, and over the bone areas in the maternal pelvis and the fetal skull of the 3D printed phantom. Approximate size of ROIs: maternal uterus and amniotic fluid, 13 000 pixels, maternal bones: 2250 pixels; fetal bones: 160 pixels (pixel size: 0.98×0.98 mm^2). For a comparison, the CT values were also measured in ROIs on similar positions in the original CIRS phantom.

TABLE 2 CT protocols and operational dose parameters used to expose the compound body phantom for individual measurements.

Tube voltage (kV)	Tube current (mA)	Pitch	Rotation time (s)	Field of view (mm^2)	$CTDI_{vol}$ (mGy)	*DLP* (mGy cm)
80	200	0.56	0.8	500 × 500	9.1	543
120	150	0.56	0.8	500 × 500	21.5	1300

The given $CTDI_{vol}$ and *DLP* values refer to the standard dosimetry phantom with a diameter of 32 cm.

2.3 | Thermoluminescence dosimetry

Holes with a diameter of 2 mm and depth of 7 mm were drilled into the printed phantom slices to accommodate rod-shaped TLDs, thus enabling the measurement of organ doses. The selected dimensions of the bore-holes minimize the air around the inserted TLDs but still allow comfortable insertion and removal of the TLD crystals using a precise pair of tweezers. Twenty-seven holes were located in the uterus and amniotic fluid, and nine were located in the fetal brain, three in the eyes, and 13 in residual tissues.

Rod-shaped LiF TLDs (LiF:Mg, Ti, TLD-100; Bicron-Harshaw, Cleveland, Ohio, USA) were inserted at the intended locations for each CT protocol. Considering the sensitivity of TLDs, the CT scans were repeated eight times to obtain a sufficiently high signal (at least 60 mGy). In the following, the results are expressed as dose per single CT scan.

Processing of the TLDs was performed as described in our previous study.[24] The uncertainty of the TLD measurements in the anthropomorphic phantom was estimated at 8%, covering measurement uncertainties of repeated TLD readings and systematic uncertainties owing to the energy or direction dependence of the TLDs and the calibration process using an ionization chamber.[28]

2.4 | Monte Carlo simulation of the dose distribution in virtual body models

The radiation exposure of the phantom resulting from the CT scan was simulated using two different voxel models.

First, we performed simulations on a voxelized version of the compound phantom shown in Figure 3. In the following, this model is named Shania. Voxelization was obtained using the ImageJ software starting from the CT image dataset of the acquisition at 120 kV. Thus, the finalized voxel model represents the compound phantom from the clavicles to the femur bone. Four pixels were merged to one voxel with a size of 1.95 × 1.95 × 2.5 mm^3, which results in a model with 1.6 × 10^7 voxels. As the compound phantom, Shania consists of five different tissues, namely soft tissue, maternal lung and breast, and the maternal and fetal skeleton, simulated with the compositions of tissues as provided in the literature.[29,30] Shania's organ doses were determined using the average values of the doses scored in the voxels corresponding to the locations of the TLDs in the compound phantom.

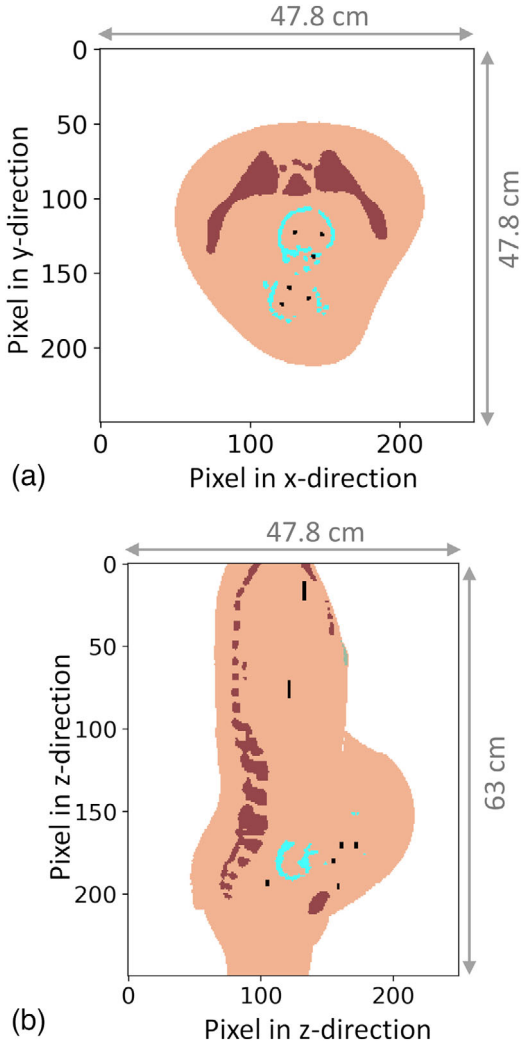

FIGURE 3 Voxel model of the compound phantom (Shania). The colors represent the individual tissues considered for simulation (light red—soft tissue, dark red—maternal bones, cyan—fetal bones, lungs and breasts are not visible in the selected sagittal slice). The positions for dose scoring, which correspond to the TLD positions in the compound phantom, are marked in black.

Second, we performed simulations on the UFPF25WK voxel model shown in Figure 4, which was used as a reference for the construction of the 3D printed abdomen. The phantom of the mother considers

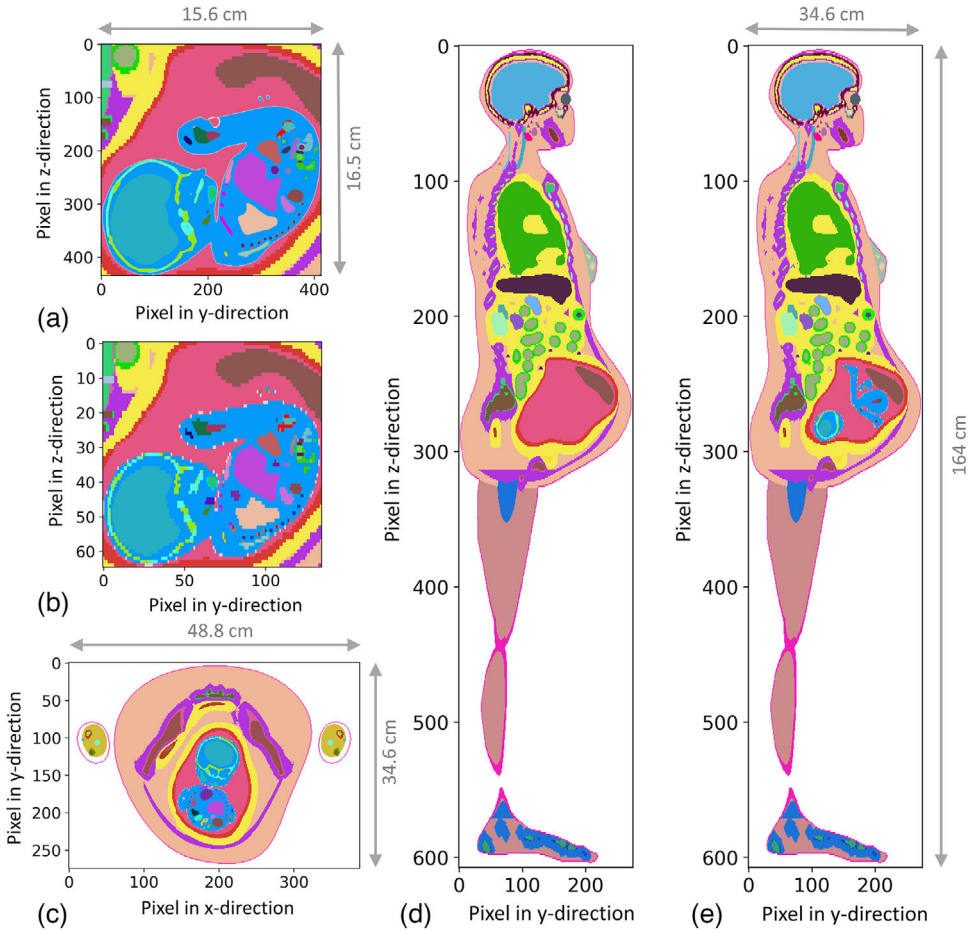

FIGURE 4 Composition of the individual UFPF25WK voxel model parts to an entire phantom of a pregnant woman. The different colors represent the individual organs, tissues, and bones (305 in total) assigned to the voxels as considered by the developers.[6] Sagittal cross sections (a, b) through the virtual model of the fetus in a high (a) and reduced spatial resolution (b). The maternal model as provided by the developers (d) contains no fetus. The sagittal (e) and transversal cross sections (c) show the combined models of the mother and the fetus as used for the Monte Carlo simulations.

200 different tissues, organs, and bones in 6×10^7 voxels with a size of $1.26 \times 1.26 \times 2.7$ mm^3. The fetus is separately modeled with 9×10^5 voxels with a size of $0.4 \times 0.4 \times 0.4$ mm^3 and consists of 105 different fetal tissues, organs, and bones. For the simulations, the voxel model of the UFPF25WK fetus (Figure 4a) was resampled to the same voxel size as in the mother model (Figure 4b) using Python 3.9.7. The scaled voxel data-set of the fetus was positioned inside the empty uterus of the mother, as shown in Figure 4c and e. All tissues were simulated with the corresponding compositions for an adult female in case of the maternal organs, and with the compositions for a newborn in case of the fetal organs, because no other data are provided in the literature yet.[30,31]

The comparison of the results obtained with the two different models (Shania and UFPF25WK) enables to investigate to which extent the dose estimates are affected by the simplifications in the diversity of the tissue compositions deriving from the inherent limitations of the 3D printing technology. Furthermore, the comparison enables also to assess the effect of the different anatomic characteristics of the UFPF25WK model compared to the 3D printed compound phantom.

The fact that some organs (e.g., fetal eyes) contain only a small number of voxels for dose scoring requires a sufficient number of simulated particles to ensure stable results with low statistical uncertainties, especially for the Shania model where doses are scored only at the TLD positions.

The simulations were performed using a Monte Carlo particle transport code based on the EGSnrc V4-2-3-0 package.[32] It was developed in previous studies and optimized for dose estimation in voxel phantoms for various irradiation geometries, including spiral scanning in a CT setup.[33,34] The energy distribution of the initial photons was set according to the energy spectrum of the CT protocols used for measurements[35] using SpekCalc.[36] The computation was performed on a Linux virtual multi-core machine (AMD EPYC 7742; AMD, Sunnyvale,

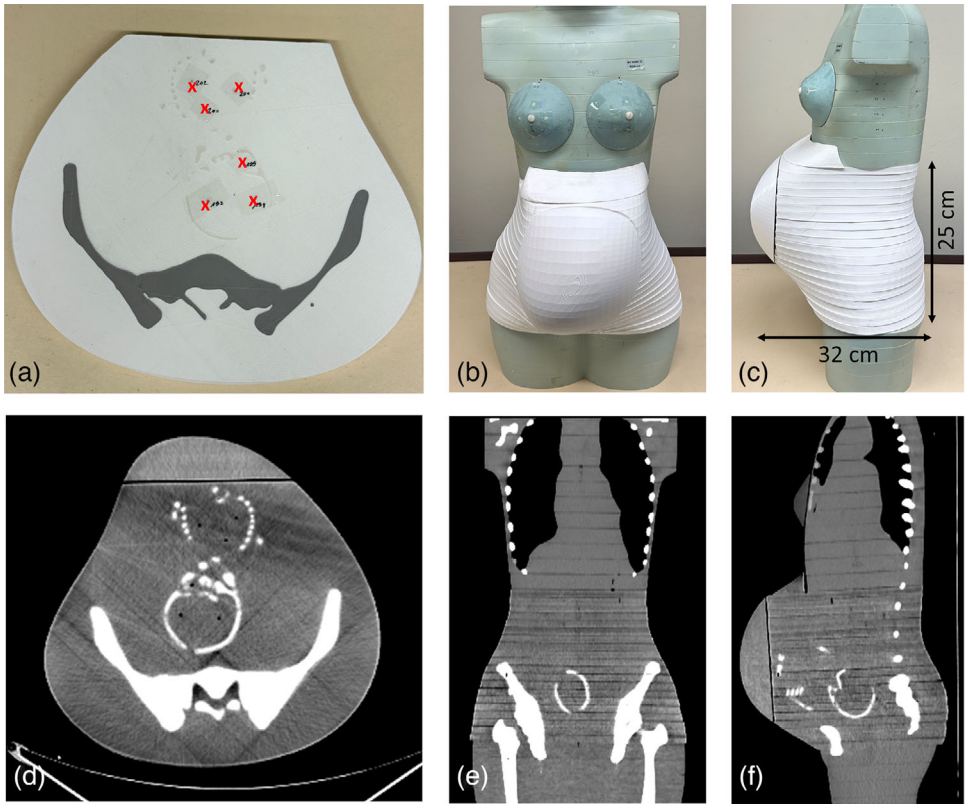

FIGURE 5 (a-c) Compound phantom of a pregnant woman consisting of the 3D printed abdomen (white parts) and the complementing parts of the CIRS phantom. Some positions for TLDs in fetal eyes, brain, and residual tissues are marked in red in the axial slice (a). (d-f) Transversal, coronal, and sagittal CT images of the compound phantom. (window settings: width 350 HU, center 40 HU, 120 kV).

California, USA) for the same body region and settings as those in the measurement. The initial number of photons was set to 10^9, resulting in coefficients of variance for the relevant organ doses lower than 3% for both models. The computation time for the simulations was 90 min.

To ensure numerical compatibility of the measured and simulated quantities, the Monte Carlo results provided as dose coefficients were scaled with the $CTDI_{vol}$ values listed in Table 2, as described in Fehrmann et al.[37] For further evaluations, the measured and simulated dose to the uterus, the amniotic fluid, and some fetal organs and body regions identified by TLD positions were compared to each other.

3 | RESULTS

The entire abdomen of the pregnant woman was printed with 18.9 kg PLA, 1.5 kg granite/PLA, and 55 g Laybrick in a total net print time of 30 days. The total cost of the print materials was 580€ (620 US$). The printing of all slices proceeded smoothly, and the materials used showed good adhesion.

Figure 5a-c shows a printed transversal slice at the level of the fetus and the frontal and lateral views of the compound phantom. The printed abdomen fits anatomically very well to the non-pregnant CIRS phantom. Therefore, the compound phantom represents a realistic approximation of a pregnant woman in the 25th week of gestation.

TABLE 3 CT values (mean ± standard deviation in HU) for the considered tissues of the 3D printed abdomen measured for the two CT protocols.

	Soft tissue	Maternal pelvis	Fetal skeleton
80 kV protocol	18 ± 30	710 ± 90	450 ± 125
120 kV protocol	18 ± 56	650 ± 77	374 ± 130

Transversal, coronal, and sagittal CT images (acquired with a tube voltage of 120 kV) of the phantom are shown in Figure 5d-f, in which the fetal skeleton is visible and distinguishable from the maternal body. The measured CT values for all tissues and protocols are summarized in Table 3. Some characteristic streak structures resulting from the printing process are visible in the soft tissue regions in the CT images. These lead to a higher standard deviation of CT values in soft tissue regions in the printed phantom as in comparable soft tissue regions of the CIRS phantom (25 ± 15 HU for 120 kV). The measured CT values agree with the corresponding CT values in humans, which range

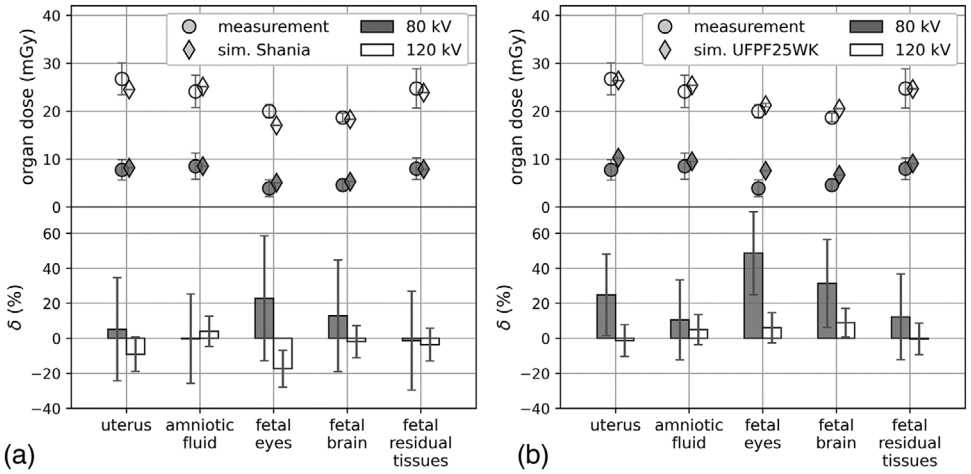

FIGURE 6 Upper parts: Organ doses in the abdomen of a pregnant woman resulting from a single CT scan as measured by TLDs in the physical phantom and simulated using the two voxel models (a. for Shania, b. for the UFPF25WK model). Lower parts: relative differences between measured and simulated organ doses. The errors for the measured values were estimated with 8%, and the error for the simulated values represents the coefficient of variance. The error bars of relative differences were determined by Gaussian error propagation.

between 10 and 40 HU for soft tissues,[38] and between 300 and 1200 HU for bones.[39] As expected, the CT values in the fetal skeleton are lower compared to the maternal bones, but no reference data of real fetal bones are available for a direct evaluation.

The measured and simulated doses in the abdominal phantom during the CT scans are plotted in Figure 6 for both voxel models.

For Shania, there is a very good agreement between simulated and measured doses for both protocols with relative differences between 1% and 13% for most of the organs; only for the fetal eyes the differences amount to about 20% (Figure 6a). However, a systematic trend was observed, with the measured dose values being overestimated for the 80-kV protocol and underestimated for the 120-kV protocol for all investigated organs.

For the UFPF25WK model (Figure 6b), there is a good agreement between the measured and simulated values for the 120-kV protocol, with the doses being identical within the uncertainties. The dose to the fetal head and the uterus was underestimated by the printed phantom in the 80-kV protocol with relative differences up to 48%.

For both models and protocols, the largest difference in these comparisons is seen in the fetal eyes, where dose is measured in only three TLDs in the compound phantom and evaluated in 83 and 428 voxels in the Shania and UFPF25WK models, respectively. Thus, an improper alignement between locations of measurement and simulation can affect the accuracy of the estimates more negatively than with other organs, which are larger and contain more TLDs.

In general, it should be consisdered that the absolute organ doses for the fetal brain and eyes are lower than for the other organs for both CT protocols.

4 | DISCUSSION

Due to the lack of commercially available anthropomorphic phantoms for patients whose stature differs markedly from that of reference persons, the possibility of producing individualized phantoms using 3D printing technologies was evaluated using the example of a pregnant woman. To this end, the abdomen of a woman in the late phase of pregnancy was printed starting from a virtual mesh model. In the following, a direct comparison of doses measured with TLDs placed inside the printed phantom and those determined by Monte Carlo simulations using two different voxel models of the pregnant woman was performed.

Measured and simulated organ doses have been compared for various non-printed anthropomorphic phantoms of non-pregnant reference persons and their digital counterparts in previous studies,[37,40–43] but such comparisons have not yet been performed for individualized 3D printed phantoms. For virtual models that represent nearly the same inner and outer anatomies as the physical phantoms, differences of up to 15% have been reported between TLD and simulation outcomes for organ doses.[42,43] In the present study, the agreement for organ doses in the abdominal region was in a similar range (between 1% and 13%, except for the fetal eyes) for Shania in both CT protocols examined.

Also for the UFPF25WK model, an excellent agreement was achieved for the 120-kV protocol, with relative differences of less than 10%. The measured dose to the fetal head was up to 50% lower for the 80-kV protocol, whereas the doses at the other positions in the abdomen agreed with the simulations also for this protocol within

the uncertainties. This model shows some differences to the 3D printed compound phantom: Firstly, there are anatomical differences regarding the width of the waist and the hips, as well as the shape of the pelvis. Second, the UFPF25WK model represents a realistic composition of a human being with different soft tissue organs, while the compound phantom considers only one homogeneous soft tissue. Third, the dose was scored in all voxels of the respective organs, while in the compound phantom, it was measured only in designated positions. However, considering the uncertainties, the relative differences of the doses calculated with the UFPF25WK model from the measurement results are comparable to those calculated for Shania, who is the voxel version of the compound phantom and therefore does not present these limitations. Therefore, it can be concluded that these factors have little influence on the doses to the abdominal organs considered for the validation process.

The good agreements demonstrate that reliable dose estimates can be obtained with individualized phantoms printed with the multi-material extrusion technology and tissue equivalent thermoplastic materials identified in our previous study.[26] On the other hand, there is a slight energy dependence of relative differences between simulated and measured organ doses for both models that is more pronounced for organs directly inside the pelvis such as the fetal head and the uterus itself. This can partly be attributed to the issue of non-ideal bone equivalent printing materials. The attenuation of the granite-composite filament used to represent a mean bone composition in the compound phantom potentially has a different energy-dependence than the bone compositions used in the simulations with the voxel models. This behavior was already shown by a comparison with cortical bone elsewhere.[26] In most cases, the present deviations still represent an acceptable approximation.

The realistic anatomy of the phantom presented in this study, including fetal structures, represents a considerable improvement compared to the simplified phantoms of pregnant women produced in previous studies.[17,19] The most important advantage is that realistic doses to specific fetal body regions can be reliably estimated, and the shielding effects of the fetal skull and the mother's pelvic bones can be properly accounted for. For instance, in this study, the dose to the fetal brain was considerably lower in both protocols than the average dose to the residual fetal body.

The CT values measured in the abdominal phantom are in the range observed in adult patients. Additionally, as expected, the CT values of the fetal skeleton are markedly lower than those of the maternal bones, which reflects the lower attenuation due to the pediatric bones having a higher cartilage content than the bones of adults.[44] However, we could not find CT values of the human fetus in the late phase of pregnancy in the literature to allow a quantitative comparison with the CT values determined for the 3D printed fetal skeleton.

This study presents some limitations:

(i) The 3D printed slices showed a recurring pattern due to the printing process, which resulted in larger standard deviations of the mean CT values compared to conventionally produced phantom slices. This must be considered when using the phantom to assess the image quality of CT scans.
(ii) The printed abdominal phantom characterizes a certain phase of pregnancy and is not representative for other phases in which the doses might be significantly different.[16,20] Moreover, in real situations, the position of the fetus is not fixed, which might have a considerable influence on the dose distribution in the fetus. However, the main aim of this study was to demonstrate the suitability of the 3D printing technique for providing realistic pregnancy phantoms. Therefore, abdominal phantoms for other gestational ages or fetal positions can be printed.
(iii) The long time required for printing the body phantom prevents the in-house production of individualized phantoms to allow fast dose estimation for individual patients in routine clinical practice. However, new printer technologies are expected to reduce the printing time and further automate printing processes.
(iv) The 3D printer used in this study had only three individual nozzles; therefore, different types of soft tissues had to be printed with the same thermoplastic material, limiting the variety of simulated tissues. For example, the ability to print fatty tissues using different materials or settings would make the phantom more realistic. Nevertheless, this approximation does not considerably affect the measured absorbed doses, as proved also in a previous study.[26]
(v) Further validation is needed to apply the phantom for measurements for radiation qualities different than those investigated in the present study, for instance, mammography or radiation therapy.

5 | CONCLUSION

Based on a detailed virtual mesh model, the abdomen of a woman in the late phase of pregnancy was successfully produced using a multi-material extrusion 3D printer. Combined with the complementary body parts of a conventionally produced anthropomorphic phantom of a non-pregnant woman, a whole-body compound phantom of a pregnant woman was constructed. As the comparison with two different voxel models with equal or similar anatomy proves, this phantom allows reliable dose measurements in fetal tissues for a large

variety of clinical exposure scenarios in diagnostic imaging. For example, it is well suited to assess in-field and out-of-field doses to the fetus resulting from intended diagnostic or interventional x-ray procedures on the mother or the effect of shielding devices intended to minimize fetal exposure. The availability of physical, individualized phantoms is of relevant importance especially for those cases that cannot be reliably reproduced by Monte Carlo simulations, for example, when tube current modulation has to be accounted for, or new CT scanner generations are entering the market, where many relevant exposure parameters are not disclosed. As the studied example of the pregnant woman demonstrates, 3D printing enables the production of phantoms of patients whose statures do not match those of commercially available body phantoms of reference individuals.

ACKNOWLEDGMENTS

The authors would like to thank Prof. Dr. Wesley Bolch and Dr. Choonsik Lee of the University of Florida for kindly providing us the datasets of the UFPF models.

CONFLICT OF INTEREST STATEMENT

The authors declare no conflicts of interest.

DATA AVAILABILITY STATEMENT

The data that support the findings of this study are available on request from the corresponding author.

REFERENCES

1. ICRP. ICRP Publication 84:Pregnancy and medical irradiation. *Annals of the ICRP*. 2000;84:30(1).
2. ICRP. ICRP Publication 60: Recommendations of the international commission on radiological protection. *Annals of the ICRP*. 1990;60:21(1-3).
3. Lowe SA. Ionizing radiation for maternal medical indications. *Prenat Diagn*. 2020;40(9):1150-1155. doi:10.1002/pd.5592
4. Horowitz DP, Wang TJC, Wuu C-S, et al. Fetal radiation monitoring and dose minimization during intensity modulated radiation therapy for glioblastoma in pregnancy. *J Neurooncol*. 2014;120(2):405-409. doi:10.1007/s11060-014-1565-4
5. Sushma N, Kaginelli S, Sathiyaraj P, Senthil Manikandan P, Ganesh KM. Analysis of fetal dose using optically simulated luminescence dosimeter and ion chamber in randophantom for various radiotherapy techniques. *Appl Radiat Isot*. 2023;198:110854. doi:10.1016/j.apradiso.2023.110854
6. Maynard MR, Long NS, Moawad NS, et al. The UF Family of hybrid phantoms of the pregnant female for computational radiation dosimetry. *Phys Med Biol*. 2014;59(15):4325.
7. Cabral MOM, Vieira JW, Neto VL, de Andrade Lima FR. Development of a pregnant woman phantom using polygonal mesh, for dosimetric evaluations. *Brazil J Radiat Sci*. 2015;3(1A).
8. Makkia R, Nelson K, Zaidi H, Dingfelder M. Hybrid computational pregnant female phantom construction for radiation dosimetry applications. *Biomed Phys Eng Express*. 2022;8(6):065015.
9. Shin B, Choi C, Nguyen TT, et al. ICRP pregnant-female mesh-type reference computational phantoms–development of maternal phantoms. *KNS 2022 Spring 춘계 학술 발표회*. 2022:1-3.
10. De Saint-Hubert M, Tymińska K, Stolarczyk L, Brkić H. Fetus dose calculation during proton therapy of pregnant phantoms using MCNPX and MCNP6.2 codes. *Radiat Meas*. 2021;149:106665. doi:10.1016/j.radmeas.2021.106665
11. Benameur Y, Tahiri M, Mkimel M, El Baydaoui R, Mesradi M. Fetal organ dose assessment during pelvic CT examination using Monte Carlo/GATE simulation and pregnancy voxelized phantom Katja. *EDP Sci*. 2022:01072.
12. Rafat Motavalli L, Hoseinian Azghadi E, Miri Hakimabad H, Akhlaghi P. Pulmonary embolism in pregnant patients: assessing organ dose to pregnant phantom and its fetus during lung imaging. *Med Phys*. 2017;44(11):6038-6046.
13. Yeom YS, Griffin KT, Mille MM, et al. Fetal dose from proton pencil beam scanning craniospinal irradiation during pregnancy: a Monte Carlo study. *Phys Med Biol*. 2022;67(3):035003.
14. Labby ZE, Barraclough B, Bayliss RA, Besemer AE, Dunkerley DAP, Howard SP. Radiation treatment planning and delivery strategies for a pregnant brain tumor patient. *J Appl Clin Med Phys*. 2018;19(5):368-374. doi:10.1002/acm2.12262
15. Gilet AG, Dunkin JM, Fernandez TJ, Button TM, Budorick NE. Fetal radiation dose during gestation estimated on an anthropomorphic phantom for three generations of CT scanners. *Am J Roentgenol*. 2011;196(5):1133-1137.
16. Matsunaga Y, Haba T, Kobayashi M, Suzuki S, Asada Y, Chida K. Fetal radiation dose of four tube voltages in abdominal CT examinations during pregnancy: a phantom study. *J Appl Clin Med Phys*. 2021;22(2):178-184.
17. Doshi S, Negus I, Oduko J. Fetal radiation dose from CT pulmonary angiography in late pregnancy: a phantom study. *Br J Radiol*. 2008;81(968):653-658.
18. Begano D, Söderberg M, Bolejko A. To use or not use patient shielding on pregnant women undergoing CT pulmonary angiography: a phantom study. *Radiat Prot Dosim*. 2020;189(4):458-465.
19. Matsunaga Y, Haba T, Kobayashi M, Suzuki S, Asada Y, Chida K. Evaluation of radiation dose for inferior vena cava filter placement during pregnancy: a comparison of dosimetry and dose calculation software. *J Appl Clin Med Phys*. 2023;24(2):e13884. doi:10.1002/acm2.13884
20. Kelaranta A, Mäkelä T, Kaasalainen T, Kortesniemi M. Fetal radiation dose in three common CT examinations during pregnancy–Monte Carlo study. *Physica Med*. 2017;43:199-206.
21. Shirkhani M, Heydarheydari S, Farshchian N, Eivazi MT, Haghparast A. Fetal dose estimation for pregnant breast cancer patients during radiotherapy using an in-house phantom. *Middle East J Cancer*. 2020;11(1):99-104.
22. Chang H-T, Liu R-W, Hsu F-Y, Hsu C-H, Lin Y-Y. Uterine dose conversion coefficients for external photons for the Taiwanese pregnant women. *Radiat Prot Dosim*. 2023.
23. Kopačin V, Brkić H, Ivković A, et al. Development and validation of the low-cost pregnant female physical phantom for fetal dosimetry in MV photon radiotherapy. *J Appl Clin Med Phys*. 2023:e14240. doi:10.1002/acm2.14240
24. Kunert P, Schlattl H, Trinkl S, et al. Reproduction of a conventional anthropomorphic female chest phantom by 3D-printing: comparison of image contrasts and absorbed doses in CT. *Med Phys*. 2023;50(8):4734-4743. doi:10.1002/mp.16587
25. Fedorov A, Beichel R, Kalpathy-Cramer J, et al. 3D Slicer as an image computing platform for the quantitative imaging network. *Magn Reson Imaging*. 2012;30(9):1323-1341. doi:10.1016/j.mri.2012.05.001
26. Kunert P, Trinkl S, Giussani A, Reichert D, Brix G. Tissue equivalence of 3D printing materials with respect to attenuation and absorption of X-rays used for diagnostic and interventional imaging. *Med Phys*. 2022;49(12):7766-7778. doi:10.1002/mp.15987
27. Schneider CA, Rasband WS, Eliceiri KW. NIH Image to ImageJ: 25 years of image analysis. *Nat Methods*. 2012;9(7):671-675.
28. Lechel U, Becker C, Langenfeld-Jäger G, Brix G. Dose reduction by automatic exposure control in multidetector computed tomography: comparison between measurement and calculation. *Eur Radiol*. 2009;19(4):1027-1034. doi:10.1007/s00330-008-1204-6

29. ICRP. ICRP Publication 23: Report of the Task Group of Reference Man. Annals of the ICRP. 1975;23.
30. Bolch W, Eckerman K, Endo A, et al. ICRP Publication 143: paediatric reference computational phantoms. *Ann ICRP*. 2020;49(1):5-297.
31. Valentin J. ICRP Publication 89: Basic anatomical and physiological data for use in radiological protection: reference values. *Ann ICRP*. 2002;32(3-4):1-277.
32. Kawrakow I, Rogers D. The EGSnrc code system. NRC Report PIRS-701. *NRC;* 2000;17:108.
33. Schlattl H, Zankl M, Becker J, Hoeschen C. Dose conversion coefficients for CT examinations of adults with automatic tube current modulation. *Phys Med Biol*. 2010;55(20):6243.
34. Schlattl H, Zankl M, Becker J, Hoeschen C. Dose conversion coefficients for paediatric CT examinations with automatic tube current modulation. *Phys Med Biol*. 2012;57(20):6309.
35. Hassan AI, Skalej M, Schlattl H, Hoeschen C. Determination and verification of the x-ray spectrum of a CT scanner. *J Med Imaging*. 2018;5(1):013506-013506.
36. Poludniowski G, Landry G, Deblois F, Evans P, Verhaegen F. SpekCalc: a program to calculate photon spectra from tungsten anode x-ray tubes. *Phys Med Biol*. 2009;54(19):N433.
37. Fehrmann M, Schegerer A, Werncke T, Schlattl H. Comparison of experimental and numerical methods of patient dose estimations in CT using anthropomorphic models. *Radiat Prot Dosim*. 2020;190(1):71-83.
38. Broder J, Preston R, Broder J. *Diagnostic Imaging for the Emergency Physician*. W.B. Saunders; 2011:1-45.
39. Kalra A. *Developing fe human models from medical images.* Basic Finite Element Method as Applied to Injury Biomechanics. Elsevier; 2018:389-415.
40. Li X, Samei E, Segars WP, et al. Patient-specific radiation dose and cancer risk estimation in CT: part I. Development and validation of a Monte Carlo program. *Med Phys*. 2011;38(1):397-407.
41. Fujii K, Nomura K, Muramatsu Y, et al. Evaluation of organ doses in adult and paediatric CT examinations based on Monte Carlo simulations and in-phantom dosimetry. *Radiat Prot Dosim*. 2015;165(1-4):166-171.
42. Struelens L, Vanhavere F, Smans K. Experimental validation of Monte Carlo calculations with a voxelized Rando–Alderson phantom: a study on influence parameters. *Phys Med Biol*. 2008;53(20):5831.
43. Long DJ, Lee C, Tien C, et al. Monte Carlo simulations of adult and pediatric computed tomography exams: validation studies of organ doses with physical phantoms. *Med Phys*. 2013;40(1):013901.
44. White D, Widdowson E, Woodard H, Dickerson J. The composition of body tissues.(II) Fetus to young adult. *Br J Radiol*. 1991;64(758):149-159.

How to cite this article: Kunert P, Schlattl H, Trinkl S, Honorio da Silva E, Reichert D, Giussani A. 3D printing of realistic body phantoms: Comparison of measured and simulated organ doses on the example of a CT scan on a pregnant woman. *Med. Phys*. 2024;51:9264–9274. https://doi.org/10.1002/mp.17420